

Observational constraints on mutated hilltop inflation

Iraj Safaei^{*}, Soma Heydari[†], Milad Solbi[‡] and Kayoomars Karami[§]

*Department of Physics, University of Kurdistan,
Pasdaran Street, P.O. Box 66177-15175, Sanandaj, Iran*

Abstract

Here, a single field inflationary model driven by a mutated hilltop potential, as a subclass of the hilltop models of inflation, is investigated. In order to constrain the parameter space of the model, the $r-n_s$ constraint of Planck and BICEP/Keck 2018 data as well as the reheating parameters such as the duration N_{re} , the temperature T_{re} , and the equation of state parameter ω_{re} , are employed. In addition, a model independent bound on the duration of the radiation dominated (RD) era N_{rd} is applied to improve the parameter space. Furthermore, the density spectra of relic gravitational waves (GWs) in light of the sensitivity domains of GW detectors, for specific inflationary durations N , are analyzed. Finally, by combining constraints from the cosmic microwave background (CMB), reheating, RD era, and relic GWs, the permissible inflationary duration is constrained to $46 \leq N \leq 56$ (95% CL) and $48.1 \leq N \leq 56$ (68% CL). Moreover, the model parameter α is confined to $0.161 \leq \alpha \leq 0.890$ (95% CL) and $0.217 \leq \alpha \leq 0.815$ (68% CL).

PACS numbers:

^{*} isafaei@kashanu.ac.ir

[†] s.heydari@uok.ac.ir

[‡] miladsolbi@gmail.com

[§] kkarami@uok.ac.ir

I. INTRODUCTION

Inflation is a well-recognized paradigm that resolves several shortcomings of the Hot Big Bang cosmology, like the horizon, flatness, and monopole problems [1–3]. During the inflation, quantum fluctuations of the inflaton field generate the scalar and tensor perturbations, which in turn produce the anisotropies observed in the cosmic microwave background (CMB). The first step in analyzing an inflationary model is to compare its predictions for the scalar spectral index n_s and the tensor-to-scalar ratio r with observational CMB data, thereby constraining the model parameters [4–6]. In the next step, one can apply the constraints on post inflationary parameters, including those associated with the reheating phase, the radiation-dominated (RD) era, and relic gravitational waves (GWs) to further refine the parameter space deduced from the CMB data.

Most inflationary models feature a potential with a flat region to sustain a slow-roll phase during the evolution of the inflaton field. After the end of inflation, the inflaton rolls down the potential and enters an oscillatory phase around the potential minimum. This oscillatory phase, known as the reheating epoch, connects the inflationary era to the RD era [7–14]. During reheating, the inflaton decays into standard model particles that results in thermalizing the Universe. The reheating phase is characterized by three parameters such as the duration N_{reh} , the temperature T_{re} , and the equation of state parameter ω_{re} . These parameters are often used to further constrain inflationary model. Following the reheating phase, the RD era begins in the evolution of the Universe. The reheating parameters influence the duration of the RD era N_{rd} . Hence, model independent bounds on the duration of the RD era provide additional constraints on the parameter space of the inflationary models [14].

A further method to constraining the inflationary models is to employ relic GWs [5, 6]. The relic GWs are generated from quantum fluctuations of the inflaton field during the inflationary era. They propagate through space-time and carry valuable information about the physics of the early Universe, owing to their non-interacting essence. The density parameter spectrum of these relic GWs is affected by the post inflationary equation of state parameter ω_{re} [7], which, consequently, depends on the model parameters. Therefore, the relic GWs serve as a powerful tool for further refining the parameter space obtained from the implications of the reheating and RD eras.

Among the multifarious inflationary models, hilltop inflation has drawn significant interest from the scientific community, due to its compatibility with small field inflation scenarios, that are in consistency with observations [12]. In recent years, variants of hilltop inflation with non-polynomial modifications, such as the mutated hilltop model, have been introduced to enhance the pliability and applicability of this framework. The mutated hilltop model, rooted in supergravity [15], incorporates a scalar potential with a hyperbolic secant term. In this model, transitions between small field and large field inflationary regimes are modulated by the parameter α [16–18]. This tunable characteristic makes the mutated hilltop model suitable for exploring observational constraints on the inflationary parameter space. In this model, the inflaton evolves from the hilltop of the potential toward its minimum around $\phi = 0$, driving an observable inflationary era. Notably, the scalar spectral index n_s predicted by the mutated hilltop potential remains largely insensitive to the model parameter, while the tensor-to-scalar ratio r varies over a range of $10^{-4} \leq r \leq 10^{-1}$, depending on the choice of parameters [17]. This range confirms the model versatility in addressing a wide spectrum of inflationary predictions.

The aim of this study is to examine the observational constraints on the mutated hilltop inflationary potential with a special focus on the role of the model parameter α in shaping inflationary observables. Additionally, we study the implications of the reheating and RD phases for the model predictions in order to analyzing how their key parameters N_{re} , T_{re} , ω_{re} and N_{rd} vary as functions of α . Furthermore, we assess the energy density spectrum of relic GWs and their detectability by upcoming GW observatories like BBO [19–23], DECIGO [22–26], LISA [27, 28], SKA [29–31], and PTA [32–36], providing insights into the observational prospects for testing the predictions of the mutated hilltop model.

This paper is classified as follows: In Section II, the basic outline of the mutated hilltop inflation is introduced. Section III is devoted to applying the reheating and RD constraints to the model. In Section IV, the prediction of the model for relic GWs is discussed. Finally, the main conclusions of the paper are summarized in Section V.

II. MUTATED HILLTOP INFLATION

The action for the present model is given by [2, 3]

$$S = \int d^4x \sqrt{-g} \left[\frac{R}{16\pi G} + \mathcal{L}(X, \phi) \right], \quad (1)$$

where g and R denote the determinant of the metric tensor $g_{\mu\nu}$ and the Ricci scalar, respectively. The term $\mathcal{L}(X, \phi)$ represents the Lagrangian density, where ϕ is the scalar field, and $X \equiv \frac{1}{2}g_{\mu\nu} \partial^\mu \phi \partial^\nu \phi$ is the kinetic energy term. Here, we consider a canonical Lagrangian given by

$$\mathcal{L}(X, \phi) = X - V(\phi), \quad (2)$$

where $V(\phi)$ is the scalar field potential. We assume the spatially flat Friedmann-Robertson-Walker (FRW) metric for $g_{\mu\nu}$ as

$$ds^2 = dt^2 - a^2(t) (dx^2 + dy^2 + dz^2), \quad (3)$$

where $a(t)$ is the scale factor and t is the cosmic time. Thus, the kinetic term simplifies to $X = \dot{\phi}^2/2$. Additionally, the energy density ρ_ϕ and pressure p_ϕ of the scalar field corresponding to the Lagrangian (2) are given by

$$\rho_\phi = \frac{1}{2}\dot{\phi}^2 + V(\phi), \quad (4)$$

$$p_\phi = \frac{1}{2}\dot{\phi}^2 - V(\phi). \quad (5)$$

Using Eqs. (4) and (5), the equation of state parameter is defined as $\omega_\phi \equiv p_\phi/\rho_\phi$. Furthermore, taking the variation of the action (1) with respect to the metric (3) yields the first and second Friedmann equations as follows

$$H^2 = \frac{1}{3M_p^2} \rho_\phi, \quad (6)$$

$$\dot{H} = -\frac{1}{2M_p^2} (\rho_\phi + p_\phi), \quad (7)$$

where $H \equiv \dot{a}/a$ is the Hubble parameter, $M_p \equiv 1/\sqrt{8\pi G}$ is the reduced Planck mass, and the dot denotes the derivative with respect to t . Moreover, the equation of motion for the scalar field, derived by varying the action (1) with respect to ϕ , is given by

$$\ddot{\phi} + 3H\dot{\phi} + V'(\phi) = 0, \quad (8)$$

where $(')$ indicates the derivative with respect to ϕ . In what follows, the first and second slow-roll parameters are defined as

$$\epsilon_{\text{H}} \equiv -\frac{\dot{H}}{H^2}, \quad (9)$$

$$\eta_{\text{H}} \equiv -\frac{\ddot{\phi}}{H\dot{\phi}}. \quad (10)$$

During the slow-roll phase, the conditions $(\epsilon_{\text{H}}, \eta_{\text{H}}) \ll 1$ are satisfied. Under the slow-roll conditions, the background Eqs. (6) and (8) can be simplified to

$$H^2 \simeq \frac{1}{3M_{\text{p}}^2} V(\phi), \quad (11)$$

$$3H\dot{\phi} + V'(\phi) \simeq 0. \quad (12)$$

Consequently, the slow-roll parameters can be rewritten as

$$\epsilon_{\text{H}}(\phi) \simeq 2M_{\text{p}}^2 \left(\frac{H'(\phi)}{H(\phi)} \right)^2, \quad (13)$$

$$\eta_{\text{H}}(\phi) \simeq 2M_{\text{p}}^2 \left(\frac{H''(\phi)}{H(\phi)} \right). \quad (14)$$

It is well recognized that the evolution of scalar and tensor perturbations can be characterized by their respective power spectra denoted by \mathcal{P}_{s} and \mathcal{P}_{t} . Under the slow-roll conditions, they can be approximated at the time of horizon exit $k = aH$ as follows

$$\mathcal{P}_{\text{s}} \simeq \frac{H^2}{8\pi^2 M_{\text{p}}^2 \epsilon_{\text{H}}} \Big|_{k=aH}, \quad (15)$$

$$\mathcal{P}_{\text{t}} \simeq \frac{2H^2}{\pi^2 M_{\text{p}}^2} \Big|_{k=aH}. \quad (16)$$

The value of the scalar power spectrum at the pivot scale $k_* = 0.05 \text{ Mpc}^{-1}$ has been estimated by Planck measurements as $\mathcal{P}_{\text{s}}(k_*) = 2.1 \times 10^{-9}$ [37]. Utilizing Eqs. (13)-(16), the scalar and tensor spectral indices in terms of the slow-roll parameters are calculated as

$$n_{\text{s}} - 1 \equiv \frac{\text{d} \ln \mathcal{P}_{\text{s}}}{\text{d} \ln k} = -4\epsilon_{\text{H}} + 2\eta_{\text{H}}, \quad (17)$$

$$n_{\text{t}} \equiv \frac{\text{d} \ln \mathcal{P}_{\text{t}}}{\text{d} \ln k} = -2\epsilon_{\text{H}}. \quad (18)$$

In addition, the tensor-to-scalar ratio is given by

$$r \equiv \frac{\mathcal{P}_{\text{t}}}{\mathcal{P}_{\text{s}}} = 16\epsilon_{\text{H}}. \quad (19)$$

Note that from Eqs. (18) and (19), the consistency relation is obtained as

$$r = -8n_t. \quad (20)$$

The Planck 2018 TT, TE, EE + LowE + Lensing + BK18 + BAO measurements impose the following constraints on n_s and r [37, 38]

$$n_s = 0.9653^{+0.0041+0.0107}_{-0.0041-0.0083},$$

$$r < 0.036. \quad (21)$$

Here, we focus on the mutated hilltop potential for our model in light of the latest observational constraints. This potential can be considered as a variant of the broader, well-known hilltop inflationary potentials. The term mutated indicates that the potential deviates from the standard hilltop form and incorporates features from hybrid inflation scenarios. In this model, inflation occurs as the inflaton rolls down the hilltop of the potential, located at small values of ϕ . The mutated hilltop potential is known to drive a more consistent inflationary era with observational data compared to the standard hilltop potentials. The mutated hilltop potential is given by [16–18]

$$V(\phi) = V_0 [1 - \text{sech}(\alpha\phi)], \quad (22)$$

where V_0 and α are constant parameters with dimensions of M^4 and M^{-1} , respectively. Using Eqs. (11) and (22), the slow-roll parameters (13) and (14) take the following forms

$$\epsilon_H(\phi) \simeq \frac{M_p^2 \alpha^2 \text{sech}^2(\alpha\phi) \tanh^2(\alpha\phi)}{2[1 - \text{sech}(\alpha\phi)]^2}, \quad (23)$$

$$\eta_H(\phi) \simeq \frac{-M_p^2 \alpha^2 \text{sech}(\alpha\phi)}{2} [2 + 3 \text{sech}(\alpha\phi)]. \quad (24)$$

Within the slow-roll approximation, inflation ends when one of the slow-roll conditions is violated. In this model, it has been demonstrated that for $\alpha > \alpha_{\text{eq}}$, $|\eta_H|$ exceeds one before ϵ_H . Consequently, the end of inflation is determined by the condition where either $\epsilon_H = 1$ or $|\eta_H| = 1$ is first satisfied [17]. Here, α_{eq} indicates the values of α at which $\epsilon_H = 1$ and $|\eta_H| = 1$ are simultaneously satisfied. Note that the scalar field value at the end of inflation serves as a boundary condition for solving the background equation (12).

Figure 1 illustrates evolutions of the scalar field, the Hubble parameter and the slow-roll parameters (23)-(24) in terms of the e -fold number N for different values of α . Here, we

utilize the e -fold definition $dN = -Hdt$, and set the end of inflation at $N = 0$. Figures 1(a) and 1(b) show that (i) for a given α , both the scalar field ϕ and the Hubble parameter H decrease when the e -fold number N decreases; (ii) for a given N , when the parameter α increases then ϕ and H decrease. Figures 1(c) and 1(d) illustrate that for $\alpha = \alpha_{\text{eq}} \simeq 0.83$, we have $\epsilon_{\text{H}} = |\eta_{\text{H}}| = 1$ at the end of inflation $N = 0$. Besides, for $\alpha > \alpha_{\text{eq}}$ the condition of end of inflation is provided by $|\eta_{\text{H}}| = 1$ which occurs before $\epsilon_{\text{H}} = 1$.

Note that the energy scale of inflation is defined by $V_0^{1/4}$ in Eq. (22). This energy scale can be obtained by fixing the scalar power spectrum in Eq. (15) at the CMB scale ($k_* = 0.05 \text{ Mpc}^{-1}$) and using Eqs. (11) and (23). The result reads

$$V_0^{1/4} = M_{\text{p}} \left(\frac{12\pi^2 \alpha^2 \mathcal{P}_s(k_*) \sinh(\alpha\phi_*) \tanh(\alpha\phi_*)}{[\cosh(\alpha\phi_*) - 1]^3} \right)^{1/4}, \quad (25)$$

where ϕ_* is the value of scalar field at the horizon exit. For the range of the parameter $\alpha \sim \mathcal{O}(0.1 - 1)$ considered in the present work, from Eq. (25) we estimate the energy scale of inflation as $V_0^{1/4} \sim \mathcal{O}(10^{-3})M_{\text{p}}$.

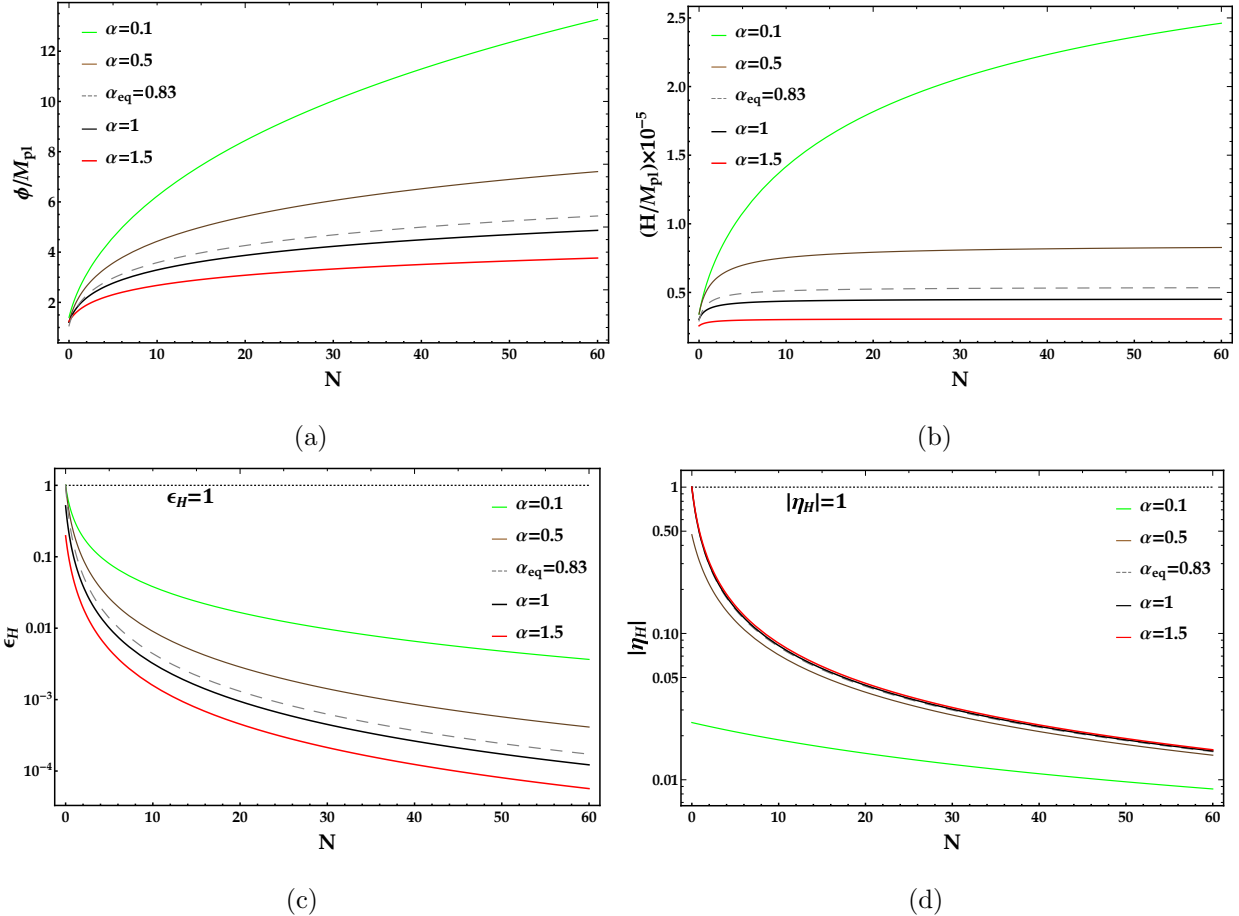


FIG. 1: Evolutions of (a) the scalar field ϕ , (b) the Hubble parameter H , (b) the first slow-roll parameter ϵ_H , and (d) the second slow-roll parameter η_H for different values of α . The green, brown, black, and red lines represent $\alpha = 0.1, 0.5, 1$ and 1.5 , respectively. Also the dashed curve in each panel corresponds to $\alpha_{\text{eq}} = 0.83$. The end of inflation is set at $N = 0$.

To assess the compatibility of the mutated hilltop inflationary model with the observational data, we constrain the model parameters using the latest observational bounds on the scalar spectral index n_s and the tensor-to-scalar ratio r given by Eq. (21). Figure 2 presents the observational $r - n_s$ panel deduced from the Planck and BICEP/Keck 2018 data as well as the prediction of the mutated hilltop model (22). Each curve in the $r - n_s$ panel corresponds to a specific e -fold number N for varying values of α from 0 at the top to 5 at the bottom along the curve. By analysis of Fig. 2, we can identify the allowed range of α for each e -fold number. For instance, for $N = 50$ (green curve), the parameter α is constrained to $\alpha \geq 0.206$ at the 95% CL, and $0.291 \leq \alpha \leq 0.815$ at the 68% CL, based on Planck 2018 TT, TE, EE + LowE + Lensing + BK18 + BAO data [37, 38]. The results

for all cases are summarized in the second column of Table I (i.e. the constraint $r - n_s$). As a consequence, applying the latest constraints from Planck and BICEP/Keck 2018 data (blue region in Fig. 2) on the model predictions for $r - n_s$ imposes a lower bound on the inflationary duration as $N = 44.4$ (95% CL) and $N = 48.1$ (68% CL) (see Table I). This implies that for $N < 44.4$ ($N < 48.1$), the prediction of model in the $r - n_s$ panel lies outside the 95% (68%) CL of the Planck and BICEP/Keck 2018 data. To explore the possibility of more constraining the parameter space, we will examine the implications of the reheating and RD epochs on the model predictions in the next section.

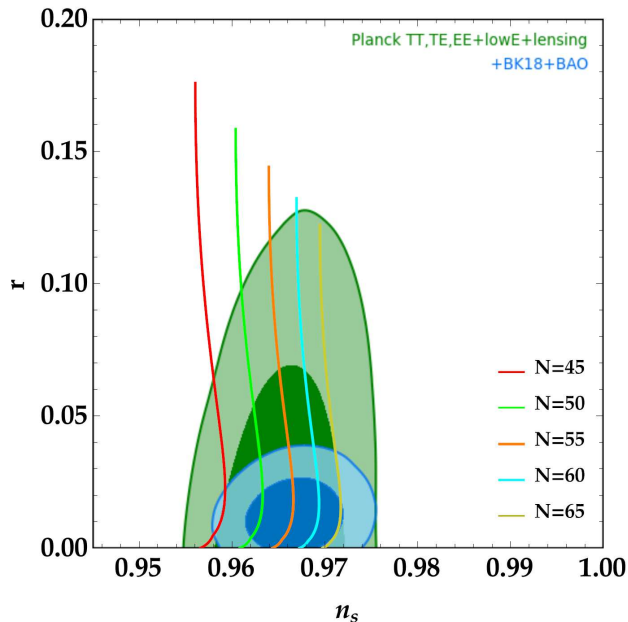


FIG. 2: The tensor-to-scalar ratio r versus the scalar spectral index n_s for varying α and different e -fold numbers N . The red, green, orange, blue, and yellow curves correspond to $N = 45, 50, 55, 60$ and 65 , respectively. The dark (light) green area represents the 68% (95%) CL of Planck 2018 TT, TE, EE + LowE + Lensing, while the dark (light) blue area shows the 68% (95%) CL of Planck 2018 TT, TE, EE + LowE + Lensing + BK18 + BAO (Planck and BICEP/Keck 2018 data) in the background. The value of the parameter α varies from 0 at the top to 5 at the bottom along each curve.

TABLE I: The allowed ranges for the α parameter related to the permitted e -fold numbers N in the mutated hilltop inflationary model, considering a combination of various constraints from Planck and BICEP/Keck 2018 data ($r - n_s$), reheating ($\omega_{\text{re}} + N_{\text{re}} + T_{\text{re}}$), RD era (N_{rd}), and relic GWs.

N	$(r - n_s)$		$(r - n_s) + \omega_{\text{re}} + N_{\text{re}} + T_{\text{re}} + N_{\text{rd}}$		$(r - n_s) + \omega_{\text{re}} + N_{\text{re}} + T_{\text{re}} + N_{\text{rd}} + \text{GWs}$	
	α (95% CL)	α (68% CL)	α (95% CL)	α (68% CL)	α (95% CL)	α (68% CL)
44.4	[0.372, 0.642]	—	[0.372, 0.642]	—	—	—
45	[0.326, 0.758]	—	[0.326, 0.758]	—	—	—
46	[0.282, 1.179]	—	[0.282, 1.179]	—	[0.779, 0.890]	—
48.1	$\alpha \geq 0.233$	[0.410, 0.490]	[0.233, 1.485]	[0.410, 0.490]	[0.362, 0.855]	[0.410, 0.490]
50	$\alpha \geq 0.206$	[0.291, 0.815]	[0.206, 1.485]	[0.291, 0.815]	[0.206, 0.818]	[0.291, 0.815]
55	$\alpha \geq 0.166$	$\alpha \geq 0.222$	[0.166, 1.485]	[0.222, 1.485]	[0.166, 0.721]	[0.222, 0.721]
56	$\alpha \geq 0.161$	$\alpha \geq 0.217$	[0.161, 0.522]	[0.217, 0.522]	[0.161, 0.522]	[0.217, 0.522]
57	$\alpha \geq 0.157$	$\alpha \geq 0.212$	—	—	—	—
60	$\alpha \geq 0.147$	$\alpha \geq 0.204$	—	—	—	—
65	$\alpha \geq 0.138$	[0.244, 0.695]	—	—	—	—

III. REHEATING IMPLICATIONS

Inflation is followed by a critical phase known as reheating. During this phase, the inflaton field begins to oscillate around the potential minimum and subsequently decays into standard model particles which leads to the thermalization of the Universe [7–14]. Thereafter, the Universe becomes hot enough to initiate the radiation-dominated era. The duration of the reheating epoch N_{re} is influenced by the rate of inflaton decay. Meanwhile, the reheating temperature T_{re} is sensitive to N_{re} and, consequently, depends on the inflaton decay rate as well. It is known that a longer reheating phase corresponds to a lower reheating temperature. Both N_{re} and T_{re} depend on the equation of state parameter ω_{re} through the following model

dependent relations [14]

$$N_{\text{re}} = \left(\frac{-4}{1-3\omega_{\text{re}}} \right) \left[N + \frac{1}{3} \ln \left(\frac{11g_{\text{re}}^{\text{s}}}{43} \right) + \frac{1}{4} \ln \left(\frac{30}{\pi^2 g_{\text{re}}} \right) + \ln \left(\frac{k_*}{a_0 T_0} \right) + \ln \left(\frac{\rho_e^{\frac{1}{4}}}{H_*} \right) \right], \quad (26)$$

$$T_{\text{re}} = \left(\frac{30\rho_e}{\pi^2 g_{\text{re}}} \right)^{\frac{1}{4}} e^{-\frac{3}{4}(1+\omega_{\text{re}})N_{\text{re}}}. \quad (27)$$

Here, g_{re} and g_{re}^{s} represent the relativistic degrees of freedom. For the temperature range $10 \text{ MeV} \leq T_{\text{re}} < 200 \text{ GeV}$, both g_{re} and g_{re}^{s} are generally temperature dependent and vary within the range $10.75 \leq g_{\text{re}} = g_{\text{re}}^{\text{s}} < 106.75$. However, the small effect of their temperature variations on N_{re} can be neglected [5]. Therefore, we set $g_{\text{re}} = g_{\text{re}}^{\text{s}} = 106.75$ for $T_{\text{re}} \geq 200 \text{ GeV}$. Additionally, $a_0 = 1$ is the current scale factor, $T_0 = 2.725 \text{ K}$ is the present temperature of the CMB, and $k_* = 0.05 \text{ Mpc}^{-1}$ signifies the comoving wavenumber at the pivot scale. Furthermore, $\rho_e = \rho_{\phi_e}$ represents the energy density of inflaton at the end of inflation. By using Eqs. (4) and (5) and setting $\omega_{\phi} \equiv p_{\phi}/\rho_{\phi} = -1/3$ at the end of inflation, one can obtain

$$\rho_e = \frac{3}{2}V_e, \quad (28)$$

where $V_e = V(\phi_e)$ is the potential at the end of inflation.

Moreover, H_* in Eq. (26) denotes the Hubble parameter at the pivot scale and can be estimated using Eq. (15) as follows

$$H_* = 2\pi M_{\text{p}} \sqrt{2\mathcal{P}_{\text{s}}(k_*)\epsilon_{\text{H}}(\phi_*)}, \quad (29)$$

where $\mathcal{P}_{\text{s}}(k_*) = 2.1 \times 10^{-9}$ is the amplitude of scalar power spectrum at the CMB pivot scale. As for the equation of state parameter ω_{re} appeared in Eq. (26), the range of $-1/3 \leq \omega_{\text{re}} \leq 1$ is considered during the reheating epoch [12]. The lower bound $\omega_{\text{re}} = -1/3$ arises from the end of inflation condition, i.e., $\epsilon_{\text{H}} = 1$, while the upper bound $\omega_{\text{re}} = 1$ represents the most conservative limit derived from causality considerations. Given the broad range of possible values for ω_{re} , it is challenging to accurately constraining the model parameter space. So, the validity of the model predictions could be compromised. In order to enhance the reliability of our model, we seek to establish a correlation between ω_{re} and the free parameter α . As demonstrated in [10], this correlation can be estimated as follows

$$1 + \langle \omega_{\phi} \rangle = 2 \left[\int_0^{\phi_{\text{m}}} d\phi \left(1 - \frac{V(\phi)}{V(\phi_{\text{m}})} \right)^{\frac{1}{2}} \right] \left[\int_0^{\phi_{\text{m}}} d\phi \left(1 - \frac{V(\phi)}{V(\phi_{\text{m}})} \right)^{-\frac{1}{2}} \right]^{-1}, \quad (30)$$

where $\langle\omega_\phi\rangle$ denotes the average value of the equation of state parameter over an oscillation cycle, which is equivalent to the reheating equation of state parameter, i.e., $\langle\omega_\phi\rangle = \omega_{\text{re}}$. Additionally, the parameter ϕ_m represents the maximum value of the scalar field during that cycle. We integrate Eq. (30), numerically, and present the result in Fig. 3. The horizontal dashed line in this figure indicates the lower bound of the reheating equation of state parameter $\omega_{\text{re}} = -1/3$. Our calculations from Eq. (30) reveal that this lower bound corresponds to $\alpha = 1.485$, which is considered as the maximum value of α . Furthermore, it can be seen from Fig. 3 that due to the positivity of α , the maximum value of ω_{re} approaches zero. Hence, the equation of state parameter in our model is constrained to the range $-1/3 \leq \omega_{\text{re}} < 0$ which results in an upper bound on the α parameter as $\alpha \leq 1.485$. Note that the shaded regions in gray, are excluded due to $\omega_{\text{re}} < -1/3$.

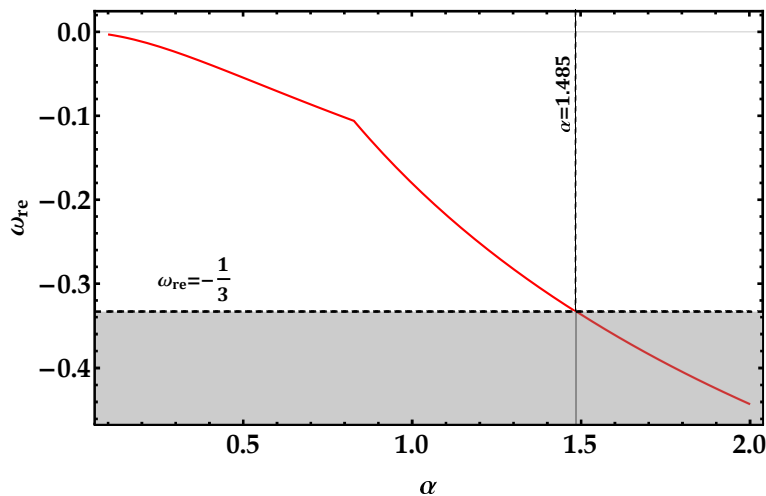


FIG. 3: Variation of the equation of state parameter, ω_{re} , versus the model parameter, α . The lower bound of ω_{re} at $-1/3$ is shown as a horizontal dashed line, while the upper bound of α at 1.485 is denoted by a vertical line. The shaded region represents disallowed values of ω_{re} .

Now, utilizing this model dependent approach in Eqs. (26)-(30), we can compute the length and temperature of the reheating period as functions of α . Figures 4(a) and 5(a) illustrate variations of N_{re} and T_{re} with respect to n_s for different values of α . Note that the length of reheating period cannot be negative, i.e. $N_{\text{re}} \geq 0$. Furthermore, as demonstrated in [14], a model independent correlation exists between the reheating parameters, which is

given by

$$N_{\text{re}}^{\text{MIB}} = \ln \left[\frac{\left(\frac{43}{11g_{\text{re}}^s} \right)^{\frac{2}{3}} \pi \sqrt{\mathcal{P}_s(k_*)} r T_0^2}{\sqrt{2} H_0 \sqrt{\Omega_{r_0}} T_{\text{re}}^2} \right]^{\frac{2}{3(1+\omega_{\text{re}})}}, \quad (31)$$

where the superscript "MIB" signifies that this is a model independent bound. Also g_{re}^s is the number of relativistic degrees of freedom in entropy at the reheating epoch. The value of g_{re}^s is typically considered to be 10.75 for low temperatures around $T_{\text{re}} = 10$ MeV, and 106.75 for $T_{\text{re}} \geq 200$ GeV [14]. In addition, $\Omega_{r_0} = 2.47 \times 10^{-5} h^{-2}$, $T_0 = 2.725$ K and $H_0 = 67.4$ Km s⁻¹ Mpc⁻¹ are the current values of the radiation density parameter, the CMB temperature and the Hubble parameter, respectively [39]. Furthermore, in Eq. (31) we set the tensor-to-scalar ratio as $r = r_{\text{max}} = 0.036$ [38].

In the model independent approach [14], the constraint on the reheating temperature reads

$$10 \text{ MeV} \leq T_{\text{re}}^{\text{MIB}} \leq 5 \times 10^{15} \text{ GeV}, \quad (32)$$

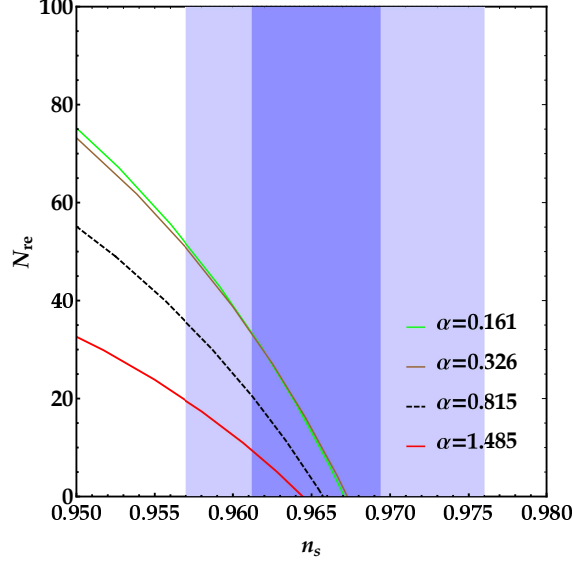
where the lower bound comes from the Big Bang Nucleosynthesis (BBN) constraint. Also the upper limit is obtained by setting $N_{\text{re}} = 0$ and $g_{\text{re}}^s = 106.75$ in Eq. (31), which is interestingly independent of ω_{re} .

Now, by substituting $T_{\text{re}}^{\text{min}} = 10$ MeV and $g_{\text{re}}^s = 10.75$ in Eq. (31), we can derive an upper bound for N_{re} as a function of ω_{re} which is plotted as a light green region in Fig. 4(b). In other words, this region is shaded between two curves including $N_{\text{re}} = 0$ (for $T_{\text{re}}^{\text{max}} = 5 \times 10^{15}$ GeV) and N_{re} as a function of ω_{re} (for $T_{\text{re}}^{\text{min}} = 10$ MeV). Furthermore, Fig. 4(b) illustrates variation of N_{re} versus ω_{re} for different values of the inflationary durations N according to Table I. It is inferred from this figure that (i) $N = 60$ (blue curve) and $N = 65$ (yellow curve) are ruled out due to their relevant negative duration of reheating $N_{\text{re}} < 0$; (ii) $N = 56$ (pink curve) is allowed for the duration of inflation only within $-0.058 \leq \omega_{\text{re}} < -0.008$; (iii) the allowed range for the duration of inflation constrained to $44.4 \leq N \leq 56$ (95% CL) and $48.1 \leq N \leq 56$ (68% CL) (see the third column of Table I); and (iv) $\omega_{\text{re}} = 0$ imposes a severe constraint on the reheating duration as $0 \leq N_{\text{re}} \leq 55.4$ compared to $0 \leq N_{\text{re}} \leq 83.1$ for $\omega_{\text{re}} = -1/3$ (see the light green region corresponding to the model independent bound in Fig. 4(b)). Therefore, we use the interval $0 \leq N_{\text{re}} \leq 55.4$ as a model independent bound in Fig. 4(c).

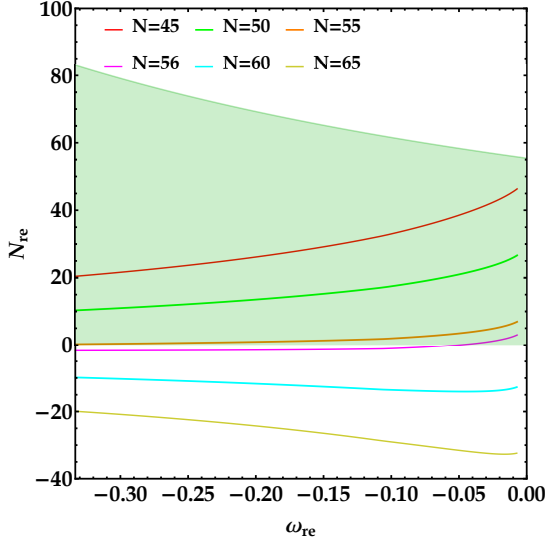
Fig. 4(c) illustrates behaviour of N_{re} as a function of α for different values of N according

to Table I. In this figure, the solid (dashed) lines represent the allowed range of α at the 95% (68%) CL for different e -fold numbers N . By analyzing this figure, we can identify the specific values of α that are consistent with the constraints on N_{re} for the present model. Also it is inferable from this figure that for $N = 56$, the permissible range of α is $0.161 \leq \alpha \leq 0.522$ at the 95% CL and $0.217 \leq \alpha \leq 0.522$ at the 68% CL (see the third column of Table I).

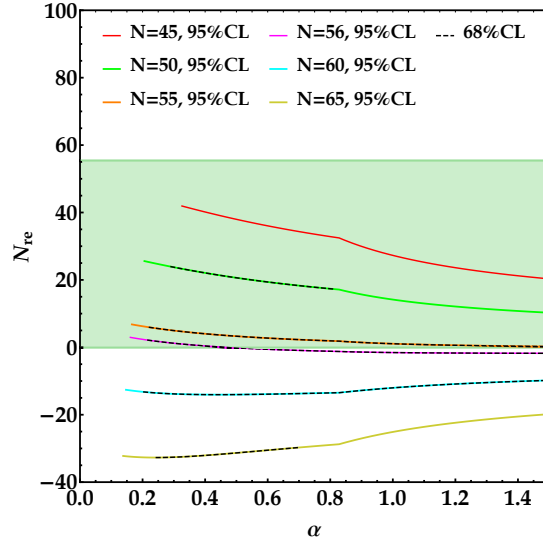
In what follows, by setting $N_{\text{re}} = 0$ in Eq. (27) which is model dependent, we calculate the maximum reheating temperature for the various values of α . The results are depicted in the legend of Fig. 5(a). The horizontal dashed line in Figs. 5(a) and 5(b) represents the model independent upper limit of the reheating temperature, $T_{\text{re}}^{\text{max}} = 5 \times 10^{15}$ GeV, while the curves illustrate the model predictions. In Fig. 5(b), behaviour of the reheating temperature T_{re} versus the α parameter for different values of N is depicted. This figure illustrates that the permitted range of α for $N = 56$ (pink curve) aligns with the previously obtained results by $N_{\text{re}} \geq 0$ (see the third column of Table I). It is obvious that, for the specific range of the α parameter in the third column of Table I, T_{re} remains below the upper bound $T_{\text{re}}^{\text{max}} = 5 \times 10^{15}$ GeV. Consequently, applying the model independent reheating constraints, Eqs. (31) and (32), imposes an upper limit on the inflationary duration in our model as $N \leq 56$ (see the third column of Table I).



(a)



(b)



(c)

FIG. 4: Variations of the reheating duration N_{re} with respect to (a) n_s , (b) ω_{re} , and (c) α . The dark (light) blue shaded region in graph (a) represents the 68% (95%) CL of the Planck 2018 TT, TE, EE + LowE + Lensing + BK18 + BAO data. The light green shaded region in the graph (b) indicates the model independent bound on N_{re} for $-1/3 \leq \omega_{\text{re}} < 0$. Also the light green shaded region in graph (c) shows the model independent bound on N_{re} for $\omega_{\text{re}} = 0$.

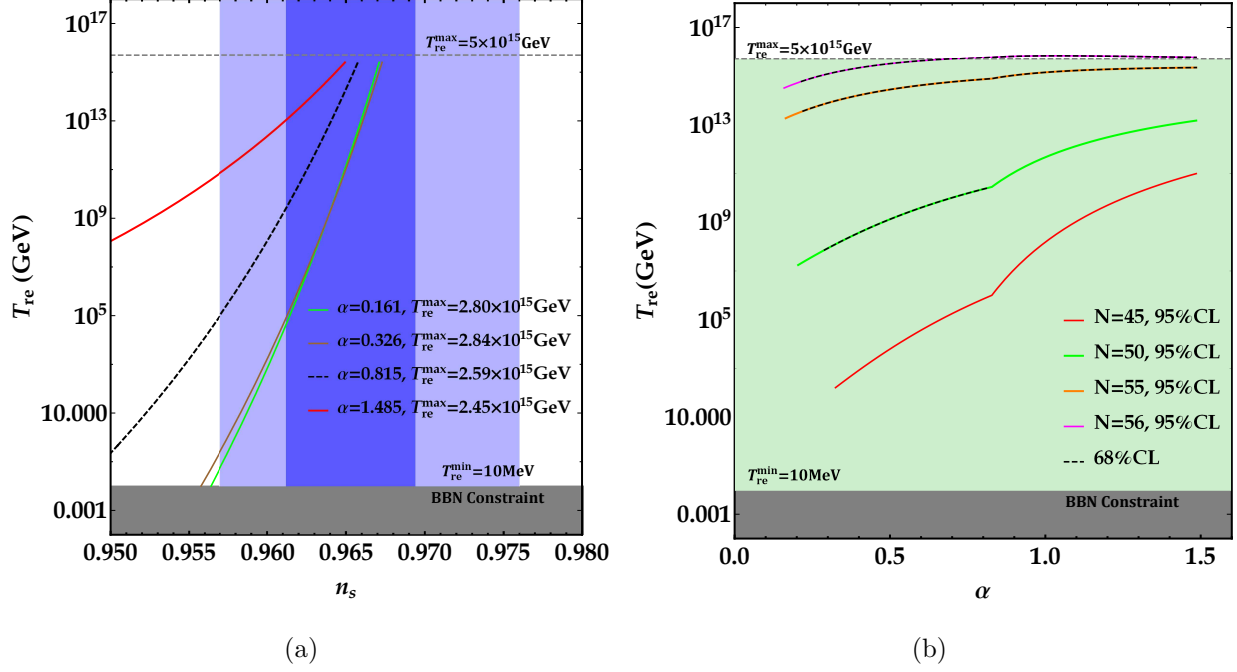


FIG. 5: Variations of the reheating temperature T_{re} versus (a) the scalar spectral index n_s , and (b) the model parameter α for different values of N . The shaded regions in graph (a) are the same as in Fig. 4(a). The light green region in graph (b) indicates the allowed range of T_{re} based on model independent constraint (32). The horizontal black dashed line at the top of each graph represents the maximum allowable reheating temperature $T_{\text{re}}^{\text{max}} = 5 \times 10^{15}$ GeV. Also the bottom hatched area corresponds to the BBN constraint.

A. Radiation dominated consideration

As previously mentioned, after thawing the Universe during the reheating epoch, the RD era is initiated. It has been shown that the reheating parameters can influence the duration of the RD era, N_{rd} , as follows [14]

$$N_{\text{rd}} = -\frac{3(1 + \omega_{\text{re}})}{4}N_{\text{re}} + \frac{1}{4} \ln \left(\frac{30}{g_{\text{re}}\pi^2} \right) + \frac{1}{3} \ln \left(\frac{11g_{\text{re}}^{\text{s}}}{43} \right) + \ln \left(\frac{a_{\text{eq}}\rho_{\text{e}}^{\frac{1}{4}}}{a_0T_0} \right), \quad (33)$$

where $a_{\text{eq}} = 2.94 \times 10^{-4}$ is the scale factor at the time of equality radiation-matter. Replacing Eqs. (26) and (30) into (33), one can numerically determine the length of the RD period as a function of α . Figure 6(a) illustrates variation of N_{rd} with respect to n_s for different values of α .

Additionally, as shown in [14], a model independent correlation exists between the reheating temperature and the length of the RD phase N_{rd} , which is given by

$$N_{\text{rd}}^{\text{MIB}} = \ln \left[\frac{a_{\text{eq}} T_{\text{re}}}{\left(\frac{43}{11g_{\text{re}}^s} \right)^{\frac{1}{3}} T_0} \right]. \quad (34)$$

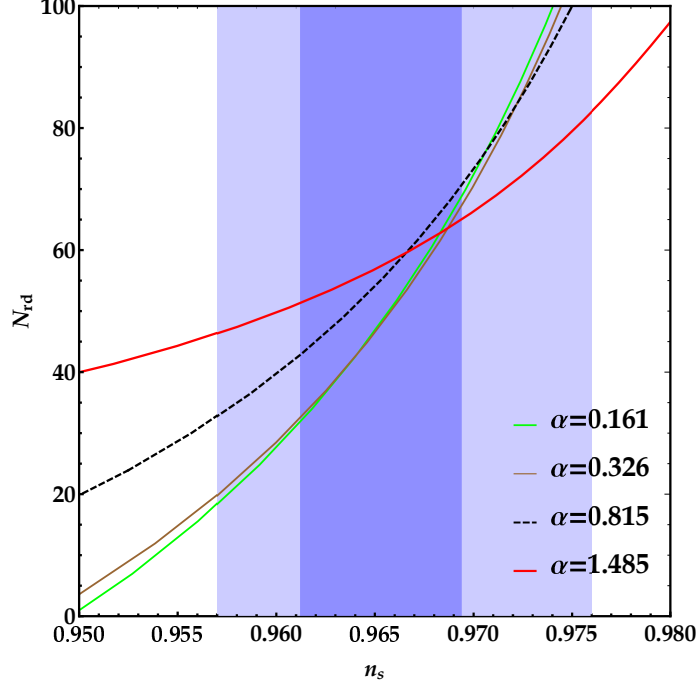
Substituting the model independent bound on the reheating temperature (32) into Eq. (34), one can determine the allowed range for the length of RD era as

$$16.7 \leq N_{\text{rd}}^{\text{MIB}} \leq 58.2, \quad (35)$$

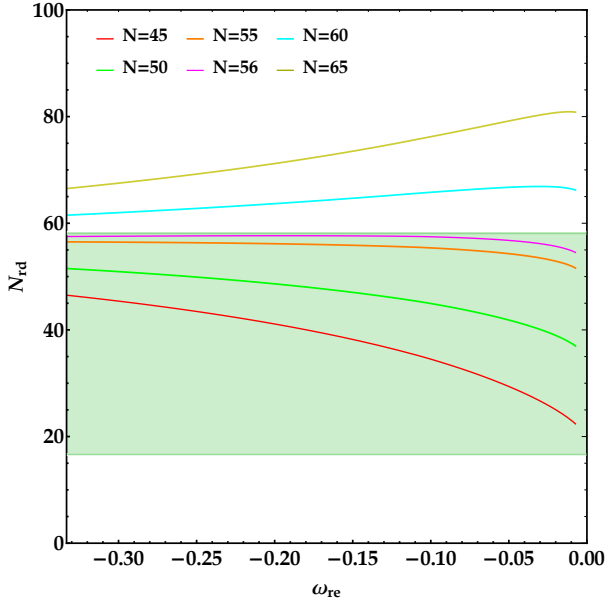
where the value of g_{re}^s is considered to be 10.75 and 106.75 for $T_{\text{re}}^{\text{min}}$ and $T_{\text{re}}^{\text{max}}$, respectively. In Figs. 6(b) and 6(c), the light green regions represent the parameter space constrained by the bound (35). As it is evident from these figures, incorporating the implications of the RD era leads to no modification of the previously estimated bounds on N and α deduced from the combined constraints $(r - n_s) + \omega_{\text{re}} + N_{\text{re}} + T_{\text{re}}$ (see again the third column of Table I).

Notably, the findings in [14] suggest a universal upper bound of 56 e -folds for observable inflation, with a maximum error of one e -fold. This aligns well with the predictions of the present model in which using a combination of constraints from CMB, reheating and RD, the inflationary duration is confined to $44.4 \leq N \leq 56$ (95% CL) and $48.1 \leq N \leq 56$ (68% CL) (see the third column of Table I).

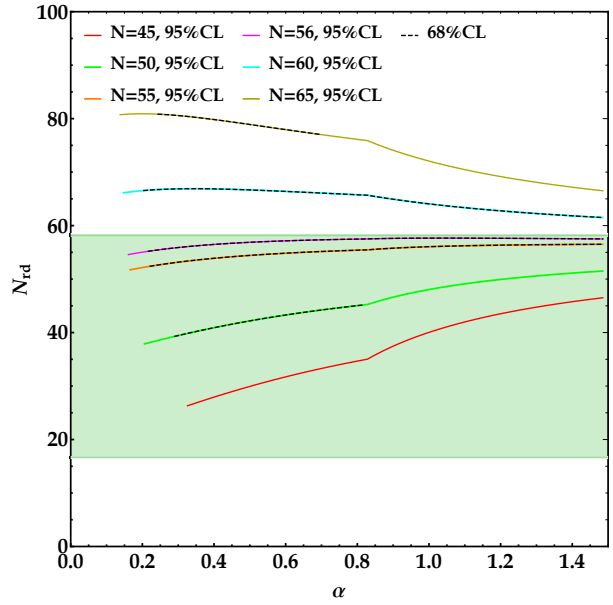
To further constrain the free parameter α of the present model, we will investigate the possibility of generating GWs in the following section. Our aim is to identify the specific range of α values that could lead to the production of GWs detectable by GW observatories.



(a)



(b)



(c)

FIG. 6: Variations of the RD duration N_{rd} with respect to (a) n_s , (b) ω_{re} , and (c) α . The shaded regions in graph (a) are the same as in Fig. 4(a). The light green shaded regions in graphs (b) and (c) indicate the model independent bound, Eq. (35).

IV. THE RELIC GRAVITATIONAL WAVES

A decisive prediction of inflation theory is the generation of relic gravitational waves. During inflation, tensor perturbations exit the horizon and subsequently re-enter after the inflationary epoch. These re-entering tensor perturbations can give rise to the propagation of GWs [5, 7, 40–44]. It is noteworthy that relic GWs offer a unique probe into the early Universe. Due to their minimal interaction with matter and radiation, they propagate undisturbed and carry valuable information about the Universe primordial conditions. The current energy density spectrum of these primordial GWs in the reheating epoch is related to its counterpart in the RD era as follows [5]

$$\Omega_{\text{GW}_0}^{(\text{re})}(f) = \Omega_{\text{GW}_0}^{(\text{RD})}(f) \left(\frac{f}{f_{\text{re}}}\right)^{2\left(\frac{\omega_{\text{re}}-1/3}{\omega_{\text{re}}+1/3}\right)}, \quad f_{\text{re}} < f \leq f_e. \quad (36)$$

Here, $\Omega_{\text{GW}_0}^{(\text{RD})}$ is the current energy density spectrum of GWs in the RD era and is given by

$$\Omega_{\text{GW}_0}^{(\text{RD})}(f) = \left(\frac{1}{24}\right) r \mathcal{P}_s(k_*) \left(\frac{f}{f_*}\right)^{n_t} \Omega_{\text{r}_0}, \quad f_{\text{eq}} < f \leq f_{\text{re}}, \quad (37)$$

where $\Omega_{\text{r}_0} = 2.47 \times 10^{-5} h^{-2}$ represents the current energy density of radiation. In addition, f_e , f_{re} , f_{eq} and f_* denote the frequencies of GWs at the end of inflation, end of reheating, matter-radiation equality, and the CMB pivot scale $k_* = 0.05 \text{ Mpc}^{-1}$, respectively. Note that in Eqs. (36) and (37), the quantities ω_{re} , r and $n_t = -r/8$ as shown in Figs. 2 and 3 can be expressed in terms of the e -fold number N and the model parameter α .

The frequency of GWs is related to the comoving wavenumber k as

$$f = \frac{1}{2\pi} \left(\frac{k}{a_0}\right). \quad (38)$$

Subsequently, it can be expressed in terms of temperature as follows [5]

$$f(T) = 7.36 \times 10^{-8} \text{ Hz} \left(\frac{g_0^s}{g_{\text{T}}^s}\right)^{\frac{1}{3}} \left(\frac{g_{\text{T}}}{90}\right)^{\frac{1}{2}} \left(\frac{T}{\text{GeV}}\right), \quad (39)$$

where $g_0^s = 3.94$ and $g_{\text{T}}^s = 106.75$ represent the effective number of relativistic degrees of freedom in entropy at the present time and at a temperature T , respectively. Additionally, $g_{\text{T}} = 106.75$ represents the effective number of relativistic degrees of freedom in energy.

To evaluate the discernibility of the predicted GWs in our model, we compute their current density spectra for the permissible ranges of α at specific e -fold numbers, $N =$

(45, 46, 48.1, 50, 55, 56). The computed results are compared with the frequency sensitivity ranges of GW detectors, as shown in Fig. 7. In this figure: (i) the colored zones illustrate the sensitivity domains of various GW detectors, such as BBO [19–23], DECIGO [22–26], LISA [27, 28], SKA [29–31], PTA [32–36], CE [45, 46], and ET [47–49]; (ii) the black (red) curve in each panel corresponds to the minimum (maximum) allowed value of α for a specific inflationary duration N according to the third column of Table I; (iii) the breaking point in the spectrum of each graph corresponds to the frequency at the end of the reheating phase, $f_{\text{re}} = f(T = T_{\text{re}})$, which from Eq. (39) it is directly linked to the reheating temperature T_{re} in Eq. (27) (see Table II); (iv) for $N = 45$, the generated GWs are not detectable by current or future GW observatories (see Fig. 7(a)); (v) for $N = (46, 48.1, 50, 55)$, we need to adjust the previously determined ranges of α in the third column of Table I to identify suitable ranges that could lead to detectable GWs by observatories (see Figs. 7(b)-7(e) as well as the last column of Table I); (vi) for $N = 46$, a narrow range of $0.779 \leq \alpha \leq 0.890$ (95% CL) is allowed for the production of detectable GWs (dashed red and blue curves in Fig. 7(b)); (vii) for $N = 48.1$, the bound on α parameter at the 95% CL should be modified to $0.362 \leq \alpha \leq 0.855$ to produce detectable GWs (see Fig. 7(c) and the last column of Table I); (viii) for $N = 50$, GWs corresponding to the lower bound of α are detectable by BBO [19–23] and DECIGO [22–26] (black curve in Fig. 7(d)). However, the upper limit on α must be modified to 0.818 (95% CL) to produce detectable GW spectrum (blue curve in Fig. 7(d)); (ix) for $N = 55$, the upper bound $\alpha = 1.485$ must be modified to 0.721 (95% and 68% CL) to produce a detectable GWs (blue curve in Fig. 7(e)); and (x) for $N = 56$, the previously determined ranges of α in the third column of Table I remain valid, and the corresponding GWs are detectable by GW observatories (see Fig. 7(f)).

Altogether, from the constraint of relic GWs, the minimum permissible duration of inflation at 95% CL is now confined to 46 e -folds with $0.779 \leq \alpha \leq 0.890$. Also, the permitted durations of inflation are obtained as $46 \leq N \leq 56$ (95% CL) and $48.1 \leq N \leq 56$ (68% CL) (see the last column of Table I).

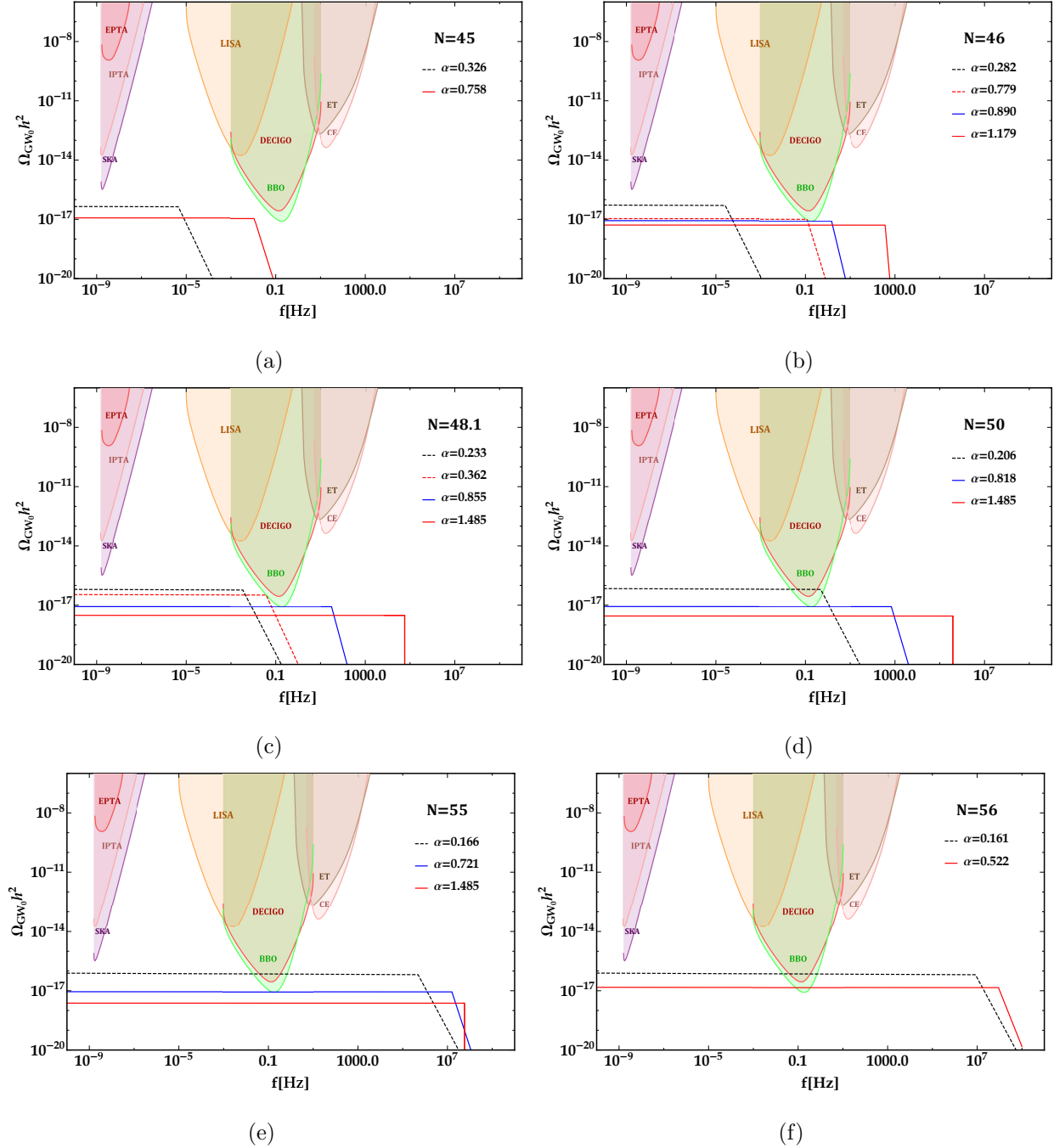


FIG. 7: The energy density spectrum of relic GWs as a function of frequency for various e -fold numbers $N = (45, 46, 48.1, 50, 55, 56)$ and their corresponding values of α . The colored regions represent the sensitivity ranges of GW detectors, including BBO [19–23], DECIGO [22–26], LISA [27, 28], SKA [29–31], PTA [32–36], CE [45, 46], and ET [47–49]. The black (red) line in each graph corresponds to the minimum (maximum) allowed values of α , according to Table I. The breaking point in the spectrum corresponds to the reheating frequency f_{re} , which is linked to the reheating temperature T_{re} listed in Table II.

TABLE II: The reheating temperature T_{re} , Eq. (27), and frequency $f_{\text{re}} = f(T = T_{\text{re}})$, Eq. (39), for various values of the e -fold number N , and the corresponding values of α . See also Fig. 5(b).

N	α	T_{re}/GeV	f_{re}/Hz
45	0.326	1.67×10^2	4.43×10^{-6}
	0.758	4.04×10^5	1.08×10^{-2}
46	0.282	9.73×10^2	2.59×10^{-5}
	0.779	4.36×10^6	1.16×10^{-1}
	0.890	5.45×10^7	1.45
	1.179	1.36×10^{10}	3.63×10^2
48.1	0.233	1.28×10^5	3.42×10^{-3}
	0.362	1.38×10^6	3.68×10^{-2}
	0.855	1.17×10^9	3.12×10
	1.485	2.17×10^{12}	5.79×10^4
50	0.206	1.75×10^7	4.68×10^{-1}
	0.818	2.57×10^{10}	6.87×10^2
	1.485	1.45×10^{13}	3.87×10^5
55	0.166	1.81×10^{13}	4.84×10^5
	0.721	5.92×10^{14}	1.58×10^7
	1.485	2.16×10^{15}	5.77×10^7
56	0.161	3.14×10^{14}	8.38×10^6
	0.217	5.87×10^{14}	1.57×10^7
	0.522	3.35×10^{15}	8.94×10^7

V. CONCLUSION

Within the framework of Einstein gravity, we studied an inflationary model driven by the mutated hilltop potential, a flexible variant of the standard hilltop potential. We demonstrated that the scalar spectral index n_s and tensor-to-scalar ratio r across different e -fold numbers N is largely compatible with the Planck constraints on the CMB data. Also, We further improve the parameter space by incorporating constraints from the reheating and RD eras. Specifically, we analyzed the reheating equation of state parameter ω_{re} , reheating

duration N_{re} , reheating temperature T_{re} , and RD duration N_{rd} , which exhibit sensitivity to α . By combining these constraints with CMB data and relic GWs, we derived the following key results:

- The mutated hilltop inflationary model aligns well with the latest observational data of $r - n_s$ from Planck and BICEP/Keck 2018, for specific ranges of N and α (see Fig. 2 and Table I).
- A minimum inflationary duration of $N = 44.4$ (95% CL) with $0.372 \leq \alpha \leq 0.642$ and $N = 48.1$ (68% CL) with $0.410 \leq \alpha \leq 0.490$ is imposed by Planck and BICEP/Keck 2018 constraints on $(r - n_s)$. See the second column of Table I.
- The reheating equation of state parameter ω_{reh} varies with α and is constrained to the range $-1/3 \leq \omega_{\text{reh}} < 0$. This imposes an upper bound on the α parameter, $\alpha \leq 1.485$ (see Fig. 3).
- Using a combination of CMB and reheating constraints, the observable inflationary duration is bounded to $44.4 \leq N \leq 56$ (95% CL) and $48.1 \leq N \leq 56$ (68% CL). The upper bound $N = 56$ is imposed by the model independent reheating condition $N_{\text{re}} \geq 0$ (see Fig. 4(c)). The model parameter α is constrained to $0.161 \leq \alpha \leq 1.485$ (95% CL) and $0.217 \leq \alpha \leq 1.485$ (68% CL).
- Constraint from duration of the RD era, N_{rd} , does not modify the estimated bounds on N and α deduced from the CMB and reheating considerations.
- Combining constraints from CMB, reheating, RD era and relic GWs, the observable inflationary duration is further refined to $46 \leq N \leq 56$ (95% CL) and $48.1 \leq N \leq 56$ (68% CL). The α parameter ranges are $0.161 \leq \alpha \leq 0.890$ (95% CL) and $0.217 \leq \alpha \leq 0.815$ (68% CL) (see the last column of Table I). The lower bound $N = 46$ and the upper bounds on α are imposed by the detectability of the relic GWs spectra (see Fig. 7).
- The predicted density spectra of relic GWs for $46 \leq N \leq 56$ fall within the sensitivity domains of various GW detectors and provide further constraints on N and α .

In summary, the mutated hilltop inflationary model is compatible with the current observational data for special ranges of N and α . Relic GWs considerations render a supplementary

layer of constraint to demonstrate the significance of combining various observational and theoretical bounds to improve the parameter space of the inflationary scenarios.

-
- [1] A. A. Starobinsky, Phys. Lett. B **91**, 99 (1980).
 - [2] A. H. Guth, Phys. Rev. D **23**, 347 (1981).
 - [3] A. D. Linde, Phys. Lett. B **108**, 389 (1982).
 - [4] M. Eshaghi, M. Zarei, N. Riazi, and A. Kiasatpour, Phys. Rev. D **93**, 123517 (2016).
 - [5] S. S. Mishra, V. Sahnia, and A. A. Starobinsky, J. Cosmol. Astropart. Phys. **05**, 075 (2021).
 - [6] I. Safaei, and K. Karami, [arXiv:2404.04872](https://arxiv.org/abs/2404.04872).
 - [7] V. Sahni, Phys. Rev. D **42**, 453 (1990).
 - [8] L. Kofman, A. D. Linde, and A. A. Starobinsky, Phys. Rev. Lett. **73**, 3195 (1994).
 - [9] J. Martin, and C. Ringeval, Phys. Rev. D **82**, 023511 (2010).
 - [10] S. Unnikrishnan, V. Sahni, and A. Toporensky, J. Cosmol. Astropart. Phys. **08**, 018 (2012).
 - [11] L. Dai, M. Kamionkowski, and J. Wang, Phys. Rev. Lett. **113**, 041302 (2014).
 - [12] J. L. Cook, E. Dimastrogiovanni, D. A. Eassona, and L. M. Kraussa, J. Cosmol. Astropart. Phys. **04**, 047 (2015).
 - [13] I. D. Gialamas, and A. B. Lahanas, Phys. Rev. D **101**, 084007 (2020).
 - [14] G. Germán, R. G. Quagliaa, and A.M. M. Colorado, J. Cosmol. Astropart. Phys. **03**, 004 (2023).
 - [15] T. Pinhero, S. Pal, Phys. Lett. B **796**, 220 (2019).
 - [16] B. Kumar Pal, S. Pal, and B. Basu, J. Cosmol. Astropart. Phys. **01**, 029 (2010).
 - [17] B. Kumar Pal, Eur. Phys. J. C **78**, 358 (2018).
 - [18] S. Yadav, D. Gangal, and K.K. Venkataratnam, Int. J. Mod. Phys. D **33**, 2450040 (2024).
 - [19] G. M. Harry et al., Class. Quant. Grav. **23**, 4887 (2006).
 - [20] J. Crowder, and N. J. Cornish, Phys. Rev. D **72**, 083005 (2005).
 - [21] V. Corbin, and N. J. Cornish, Class. Quant. Grav. **23**, 2435 (2006).
 - [22] K. Yagi, and N. Seto, Phys. Rev. D **83**, 044011 (2011).
 - [23] K. Yagi, and N. Seto, Phys. Rev. D **95**, 109901 (2017).
 - [24] S. Kawamura et al., Class. Quant. Grav. **23**, S125 (2006).
 - [25] S. Kawamura et al., Class. Quant. Grav. **28**, 094011 (2011).

- [26] N. Seto, S. Kawamura, and T. Nakamura, *Phys. Rev. Lett.* **87**, 221103 (2001).
- [27] K. Danzmann, *Class. Quant. Grav.* **14**, 1399 (1997).
- [28] P. Amaro-Seoane et al. (LISA Collaboration), [arXiv:1702.00786](#).
- [29] C. J. Moore, R. H. Cole, and C. P. L. Berry, *Class. Quant. Grav.* **32**, 015014 (2015).
- [30] C. L. Carilli, and S. Rawlings, *New Astron. Rev.* **48**, 979 (2004).
- [31] A. Weltman et al., *Publ. Astron. Soc. Aust.* **37**, e002 (2020).
- [32] J. Antoniadis et al. (EPTA Collaboration), *Astron. Astrophys.* **678**, A50 (2023).
- [33] J. Antoniadis et al. (EPTA Collaboration), *Astron. Astrophys.* **678**, A48 (2023).
- [34] J. Antoniadis et al. (EPTA Collaboration), *Astron. Astrophys.* **678**, A49 (2023).
- [35] J. Antoniadis et al. (EPTA Collaboration), *Astron. Astrophys.* **690**, A118 (2024).
- [36] J. Antoniadis et al. (EPTA Collaboration), [arXiv:2306.16227](#).
- [37] Y. Akrami et al. (Planck Collaboration), *Astron. Astrophys.* **641**, A9 (2020).
- [38] P. A. R. Ade et al. (BICEP/Keck Collaboration), *Phys. Rev. Lett.* **127**, 151301 (2021).
- [39] N. Aghanim *et al.* (Planck Collaboration), *Astron. Astrophys.* **641**, A6 (2020).
- [40] D. G. Figueroa, and E. H. Tanin, *J. Cosmol. Astropart. Phys.* **08**, 011 (2019).
- [41] N. Bernal, and F. Hajkarim, *Phys. Rev. D* **100**, 063502 (2019).
- [42] C. Caprini, and D. G. Figueroa, *Class. Quant. Grav.* **35**, 163001 (2018).
- [43] V. Sahni, M. Sami, and T. Souradeep, *Phys. Rev. D* **65**, 023518 (2001).
- [44] B. Allen, *Phys. Rev. D* **37**, 2078 (1988).
- [45] D. Reitze et al., *Bull. Am. Astron. Soc.* **51**, 035 (2019).
- [46] B. P. Abbott et al., *Class. Quant. Grav.* **34**, 044001 (2017).
- [47] M. Punturo et al., *Class. Quant. Grav.* **27**, 194002 (2010).
- [48] S. Hild et al., *Class. Quant. Grav.* **28**, 094013 (2011).
- [49] M. Maggiore et al., *J. Cosmol. Astropart. Phys.* **03**, 050 (2020).

